Prakhar Yadav[1*], Aditya Kumar Singh[2], Rakesh Kumar Singh[3], Saiyed Salim Sayeed[4], Amrees Pandey[5]

A Compact Four-Port Ultra-Wideband MIMO Antenna Employing Slot-Based Penta-Band Suppression and Centralized EBG Decoupling Network

Journal of Electrical Systems

Abstract: This study presents a small four-elements ultra-wideband (UWB) antenna system with inbuilt multi-band suppression and enhanced isolation that has a multi-input multi-output (MIMO) antenna configuration. To achieve the performance of wideband, the antenna is built based on circular monopole radiators printed on an adjusted ground plane. In order to reduce the electromagnetic interaction between the closely spaced elements, a periodic electromagnetic bandgap (EBG) structure with periodic 3×3 pattern is inserted in the center of the substrate to essentially limit the amount of surface-wave coupling. Each radiating patch has five resonant inverted U-shaped slots that form controlled rejection bands in the UWB spectrum that reject interferon of the existing wireless systems between 3.36 GHz and 5.50 GHz. Expertise experimentally shows an operating bandwidth of 3.0 to 14.0 GHz. Experimental performance indicates that the operation bandwidth is 3.0 to 14.0 GHz ($|S11| \leq -10$ dB), with an inter port isolation of more than -22.5 dB, a gain of 6.2 dB, and a radiative efficiency of approximately 79%. The design is suitable in development of small high-speed UWB-MIMO communication equipment where there is a need to have a reliable interference mitigation and low mutual coupling.

Keywords: EBG, Slotted Patch, Penta-Band, UWB, Gain, Radiation Pattern, Isolation.

1. INTRODUCTION

The allocation of 3.1-10.6 GHz frequency band to short-range high-speed wireless communication by the Federal Communications Commission (FCC) has drawn the attention of many researchers to the use of ultra-wideband (UWB) technology [1]. This regulatory license encouraged the fast advancement of compact and broadband antennas that can be used in portable and embedded wireless gadgets. Other developments have included adoption of multiple-input multiple-output (MIMO) techniques in UWB systems that have been found to be viable in improving the capacity of a channel, signal reliability, and multipath fading resistance. Although these benefits exist, close electromagnetic of radiating elements can often be an issue in making compact UWB-MIMO antennas operate effectively. Mutual coupling compromises isolation, diversity performance and radiation characteristics. Some studies have dealt with this problem by suggesting smaller MIMO designs with enhanced isolation behavior [2, 3]. Thereafter, dual-polarization and self-complementary forms also were studied to increase diversity and band-rejection properties [4], whereas fractal geometries were employed to obtain antenna miniaturization and WLAN band rejection [5]. More directions of isolation enhancement were obtained with modified ground structures, decoupling branches and parasitic components in two-port and multi-port UWB-MIMO systems [6-9]. Design principles of classical antenna design principles that control the behavior of impedance matching and radiation remain influential in these developments [10]. Other methods have also been proposed such as parasitic strips and floating decoupling structures, which enhance isolation without footprint expansion of the antenna [11, 12]. Parallel to this, uniplanar electromagnetic bandgap (EBG) structures have been used in between the antenna elements to inhibit surface-wave propagation and minimize coupling [13]. This is inspired by the metamaterial-based periodic structures that were optimized into these EBG surfaces that are effective as a means of mitigating mutual coupling in antenna systems [15]. The recent research trends have devoted to multi-port UWB-MIMO

[1]Department of Electronics & Communication, University of Allahabad, Prayagraj, India
[2]Department of Electronics and Communication Engineering, Noida Institute of Engineering and Technology (NIET), Greater Noida, India
[3,5]Department of Electronics and Communication Engineering, Shambhunath Institute of Engineering and Technology (SIET), Prayagraj, India
[4]Military college of Telecommunication Engineering, MHOW, Indore, Madhya Pradesh, India
*Corresponding Author Email: prakhar@allduniv.ac.in

antennas with multiple band-rejection properties to prevent interference with other wireless services that are co-existing. It has also been reported that spectral coexistence problems are solved by quad-port and multi-band notched designs [16,17]. High isolation dual- and triple-band UWB-MIMO antennas have also been shown to be effective at suppressing interference [18, 19]. Additionally, common diversity performance indicators, including envelope correlation coefficient (ECC) and diversity gain (DG) are popularly used to analyze the efficiency of MIMO antennas [20]. Further advances in isolation and bandwidth have been achieved by neutralization lines, characteristic mode analysis and ground protrusion [21–25]. Scalability of multi-element UWB planar arrays and compact diversity antennas has also been demonstrated by expandable arrays and compact arrays [26-28]. The antenna arrays with the concept of EBG structures in antenna arrays to suppress coupling proposed originally as an array concept [29], formed the basis of current EBG-aided decoupling. Even though significant advancement has been achieved in the design of UWB-MIMO antennas, the majority of the current designs are reduced to two or three port designs and have limited control over numerous notch bands. It has been a comparatively unexplored research question whether it is possible to develop a compact quad-port configuration which can not only be made to operate over a wide band, but also offers multiple controlled band-stop responses and high inter-element isolation. The current paper will overcome this issue by introducing a miniaturized quad-port UWB-MIMO antenna with five band-notch features which are independently controlled and an EBG-based decoupling. The design applies the elements of circular monopoles printed on a modified defected ground structure (DGS) in order to achieve full UWB coverage. The desired band-stop responses are produced by etching inverted U-shaped slots on each of the radiators. The inherent orthogonal positioning of neighboring elements inherently minimizes the coupling of perpendicular pairs, whereas the centrally located 3×3 EBG array is useful in the suppression of surface-wave interaction between parallel elements. The artificially created prototype shows operating bandwidth 3.0 to 14.0 GHz with the notch frequencies being 3.4, 3.8, 4.2, 4.7 and 5.3 GHz. The separation between any two ports is approximately 22.5 dB, which confirms the success of the proposed EBG-aided isolation design to compact multi-port UWB-MIMO systems.

2. ANTENNA CONFIGURATION AND PERFORMANCE ANALYSIS

In this section, the structural development and the working principle of the suggested quad-port UWB-MIMO antenna are explained. The antenna is designed on an inexpensive dielectric substrate, four identical radiating elements are placed in a small-scale orthogonal design in order to provide pattern diversity and spatial separation.

2.1. Methodology for Achieving Wideband Performance

The process of the progressive development of the antenna solution in question is presented in Figure 1. The antenna is designed on FR-4 with relative permittivity of 4.3, with a thickness of 1.6 mm. The main radiating structure is made of a square copper patch of 27 mm × 27 mm that is printed on the substrate. First, the design has a circular monopole element as explained in the first occupation (Case I). The simplified version of this resonates close to 3.8 GHz and has a rather narrow 3 GHz band of impedance. At this phase, a traditional rectangular ground plane of dimensions W × Lg is used. In the ground structure, modifications are brought about in order to attain ultra-wideband performance. The ground plane has a rectangular slot etched in it and the edges of the upper part are rounded off to enhance current distribution and impedance properties. These changes enable a vast improvement of matching conditions and an extension of the operational bandwidth. The adjusted structures are known as Case II and Case III and they increase the impedance bandwidth of -10 dB to 3.1 GHz all the way to 14.0 GHz and thus meet UWB requirements.

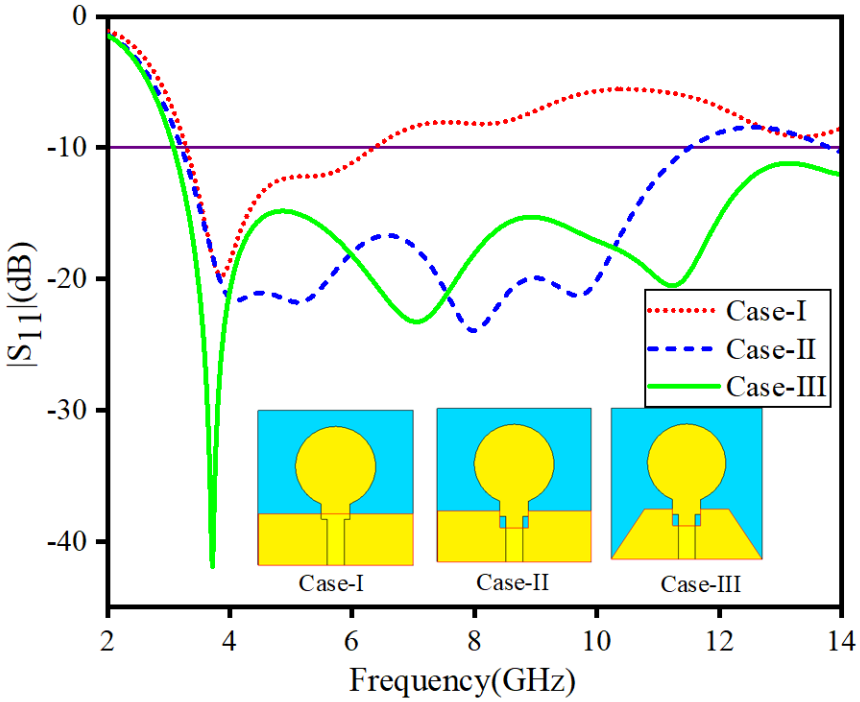

FIGURE 1. Simulated performance of structures of several evolutionary antennas in return loss.

2.2. Multi-Band Suppression Features Development.

Figure 2 shows that the ultra-wide band frequency will overlap with a number of established narrowband communication schemes, which could pose electromagnetic interference. These services encompass WiMAX, C-band satellite connections, Wi-Fi, INSAT, WLAN, and X-band application and radio navigation net. Selective band-rejection characteristics were then added to the antenna structure to avoid the performance degradation due to such coexistence as the wideband behavior of the antenna structure had been checked. To ensure that the wireless services did not interfere, 3.46 GHz, 3.82 GHz, 4.22 GHz, 4.72 GHz, and 5.34 GHz were selected as desired rejection bands as indicated in Figure 2(a). Figure 2(c) simulated reflection coefficient and VSWR plots confirm the existence of five distinct notch bands that are located in the UWB spectrum. Irrespective of the implementation of these stopbands, the antenna has continuous impedance bandwidth between 3.0 GHz and 14.0 GHz. The material size of the resonant slots that rejected each of the rejected frequencies was computed using standard resonance-based design equations as revealed below.

$$f_n^i = \frac{c_0}{2L_{\text{slot}}^i \sqrt{\varepsilon_{eff}}} \tag{1}$$

$$L_{\text{slot}}^i = 2L_i + w_i \tag{2}$$

$$\varepsilon_{eff} = \frac{\varepsilon_r + 1}{2} \tag{3}$$

2.3. Parametric Investigation

The effect of geometrical changes on frequency bands rejection is studied using parametric simulation in details. The simulated reflection coefficient responses to the adjustment of the individual notch elements are shown in figure 3. In the inverted U-shaped slots, the notch frequencies are mainly dictated by the effective parameters of length and width (L3-L7 and W3-W7). Strong currents on the surface are concentrated at the edges of the slot at the chosen frequencies of rejection. The two currents of each U-shaped slot are oppositely directed thus cancelling the fields and causing a high-impedance condition. In accordance with the resonance condition in Equation (1), the notch frequency is mainly controlled by the effective electrical length of slot resonator. The dependence of the rejected frequency on substrate properties and slot geometry is further explained by the effective wavelength relation provided in Equation (2) and the expression of effective dielectric constant provided in Equation (3). Figure 3(a)-3(e) shows the simulation of the |human| of S11 (dB) which clearly show the existence of five different

notch bands in the UWB spectrum. The parametric findings indicate that as the effective slot length is increased the respective rejection frequency decreases and conversely when the slot length decreases the notch is shifted to higher frequencies. This trend is directly proportional to the inverse of the resonant length to the resonant frequency as per the Equations (1) to (3). It is also noted that each slot primarily manages its corresponding stopband with very little interrelation with other notch components. Thus, the five rejected bands can be independently tuned by setting the physical dimensions and location of the respective slot structures properly.

2.4. Achievement of the Quad-Element MIMO Arrangement.

Figure 4(a) presents the design of the proposed four-port UWB-MIMO antenna. The building is organized into four radiating elements of the same size and placed orthogonally to the others to achieve spatial and polarization diversity in a very small area. The area occupied by each antenna element is about $0.072\lambda^2$ which is space efficient and can be fitted in integrated wireless systems. The comparison of the simulated parameters of scattering suggests that mutual coupling behavior is different based on the relative orientation of the elements. The isolation of the perpendicular antenna pairs is relatively higher because of low field overlap. The parallel element pairs (13 and 14) are however relatively more strongly coupled. Based on the S-parameter results, it can be seen that the isolation between these parallel ports is approximately -20 dB only over a limited range in terms of frequencies, in particular, between 5.0-5.21 GHz and between 7.13-8.58 GHz. Beyond these bands, the coupling level becomes greater, and it is necessary to enhance more decoupling strategies to get steady high isolation throughout the UWB range.

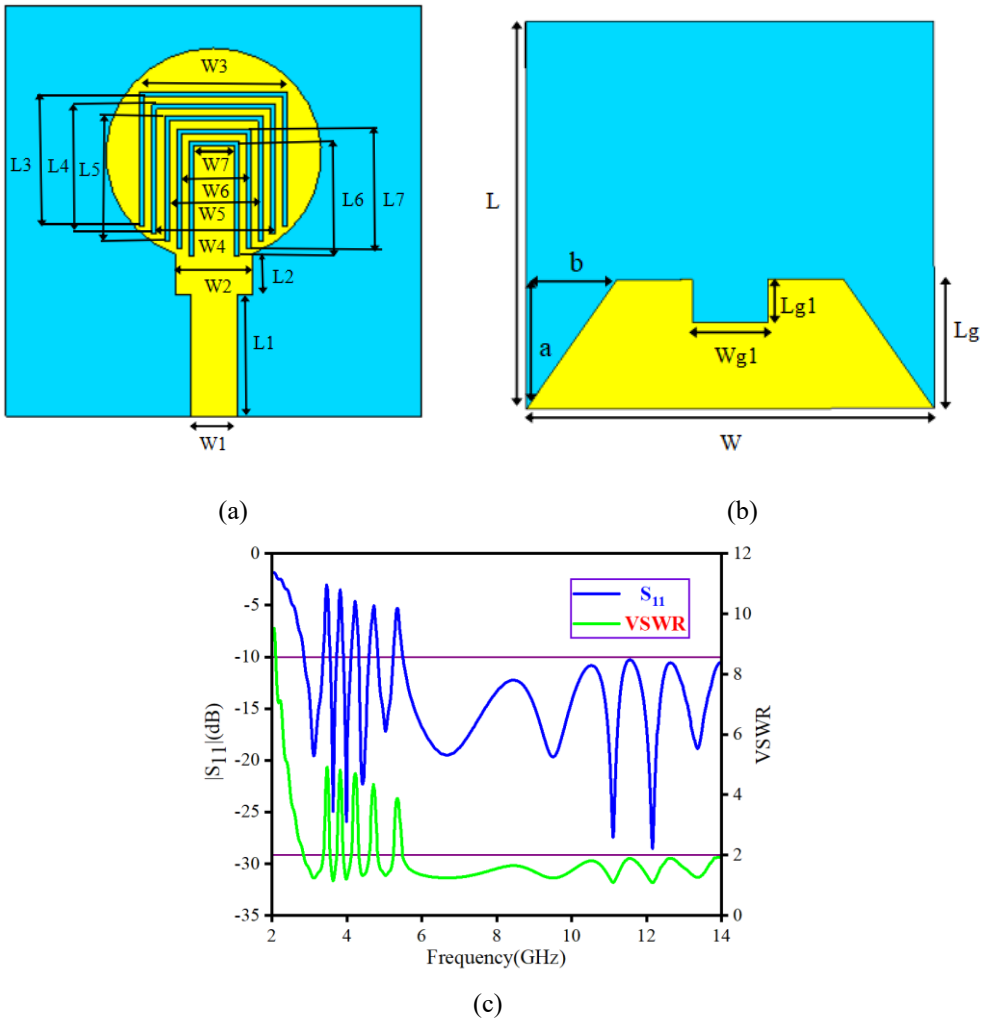

FIGURE 2. Geometry and optimum parameter of the single radiating element proposed (a) top-layer, (b) ground-layer, and (c) simulated |S11| and VSWR performance in the UWB-MIMO setup.

Optimized dimensional values (in mm): R = 7.0; W = 27.0; W1 = 3.0; W2 = 5.0; W3 = 9.6; W4 = 8.0; W5 = 6.4; W6 = 4.8; W7 = 3.2; Wg1 = 5.0; L = 27.0; L1 = 8.0; L2 = 2.7; L3 = 8.8; L4 = 8.5; L5 = 8.2; L6 = 7.9; L7 = 7.6; Lg = 9.0; Lg1 = 3.0.

On the other hand, the pair of perpendicularly (pairs 12 and 14) place the antenna elements such that their isolation level remains quite constant at about -22.5 dB over the whole band of operation. The enhanced orthogonal orientation is the main cause of this enhanced decoupling, as it has a minimum number of cross current paths and polarization similarity.

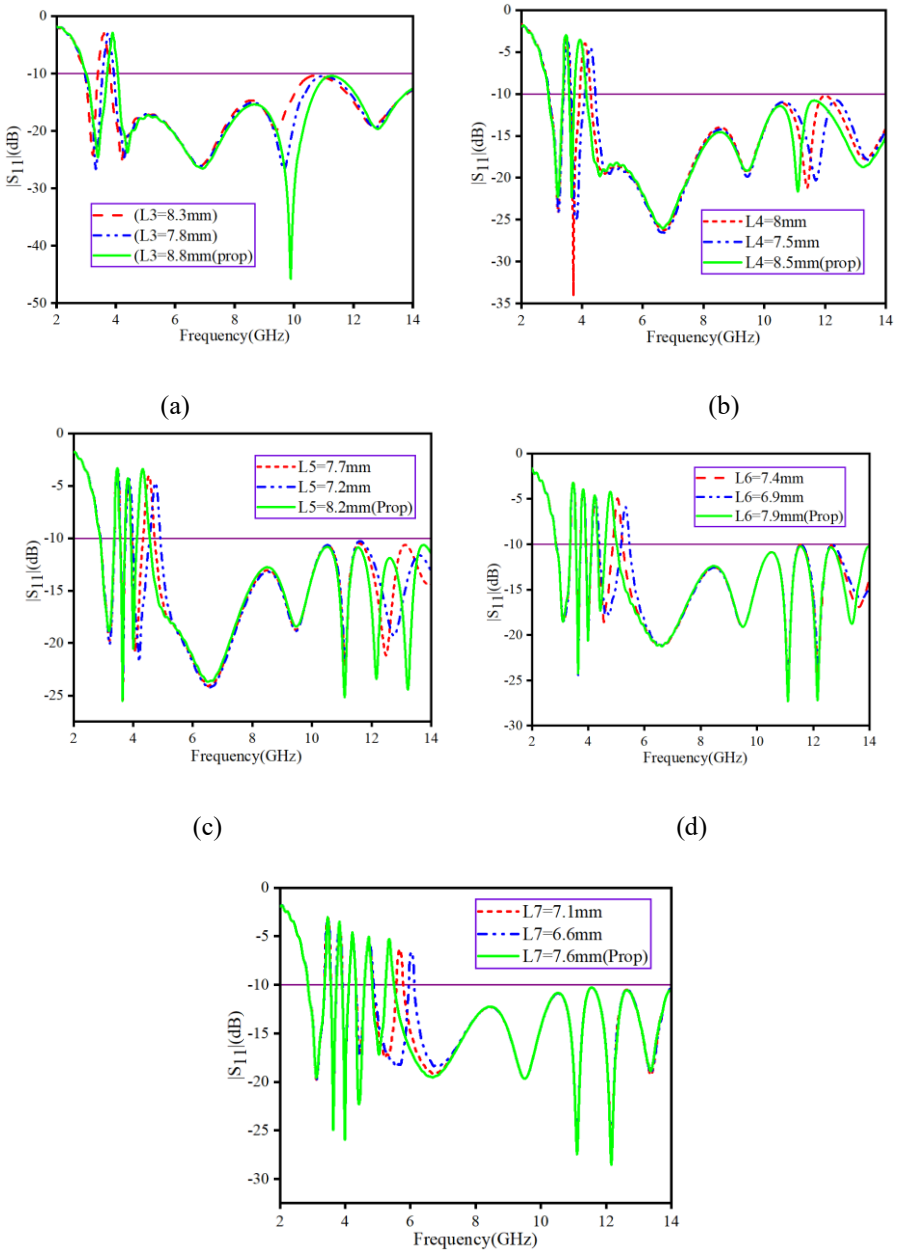

FIGURE 3. Parametric investigation of the simulated reflection coefficient (|S11|) response influence of varying (a) outermost slot length (Slot-1), (b) Slot-2 length, (c) Slot-3 length, (d) Slot-4 length, and (e) innermost slot length (Slot-5).

Conversely, they are stronger interacting in electromagnetic aspect (similar radiation patterns and polarization characteristics) and the parallel element pairs are mostly mutually coupled. To overcome this shortcoming and

improve the isolation performance in general, a periodic electromagnetic bandgap (EBG) pattern was presented between the parallel elements.

2.5. Assessment of Electromagnetic Bandgap Properties.

EBG surfaces find extensive application to prevent propagation of surface-waves and to minimize mutual coupling of small antenna systems. In order to eliminate the coupling experience in the frequency range of 5.0 to 5.21 GHz and 7.13 to 8.58 GHz, a periodic 3 x 3 EBG plating is incorporated between the parallel antenna elements. Figures 4(b)-4(e) represent the general structure of the EBG array, geometry of a single cell and optimized dimensions of a single cell and the lumped-element equivalent circuit model. The resonant LC representation is a way in which one can explain the operating mechanism of the EBG structure. In this model, the fringing electric fields between adjacent patches of metallic create the capacitance component C1, and the capacitance between each patch and the ground plane across the dielectric substrate was C2. The metallic inductive vias between the patch and the ground plane contribute to the inductance of the patch structure L. In a unit cell, characterized by patch width (W), inter-element gap (g), substrate thickness (h), and dielectric constant (εr), the effective inductance and capacitance of a cell are calculated with the help of the following analytical expressions: All of these parameters control the frequency of the bandgap and the stopband properties that cause the surface-wave inhibition.

$$c_1 = \frac{\varepsilon_0 w}{\pi} \operatorname{arch}\left(\frac{w+g}{g}\right) \tag{4}$$

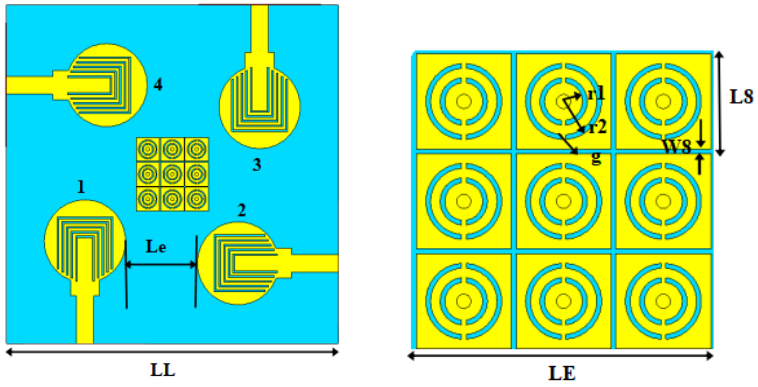

(a) (b)

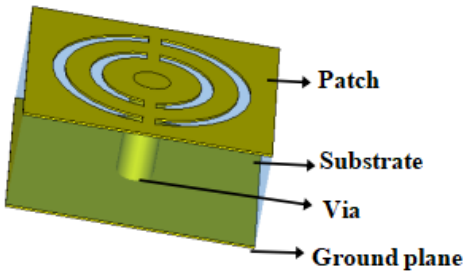

(c)

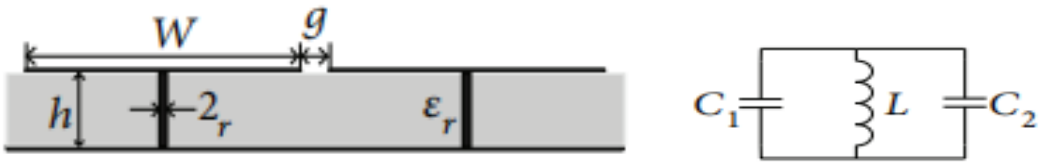

(d) (e)

FIGURE 4. Elaborate design of the proposed quad-port UWB-MIMO system and EBG integration: (a) geometry and dimensional layout of the four-element antenna, (b) layout of the 3 × 3 electromagnetic bandgap

array, (c) structural design of a unit cell in the EBG, (d) optimized dimensional parameters on the unit cell and (e) parallel LC resonant circuit representation.

All the geometric parameters are given in millimeters: LL = 54, Le = 15.3, W8 = 4, L8 = 4, g = 0.2, LE = 12.4, h = 1.6, r1 = 0.8, and r2 = 1.6.

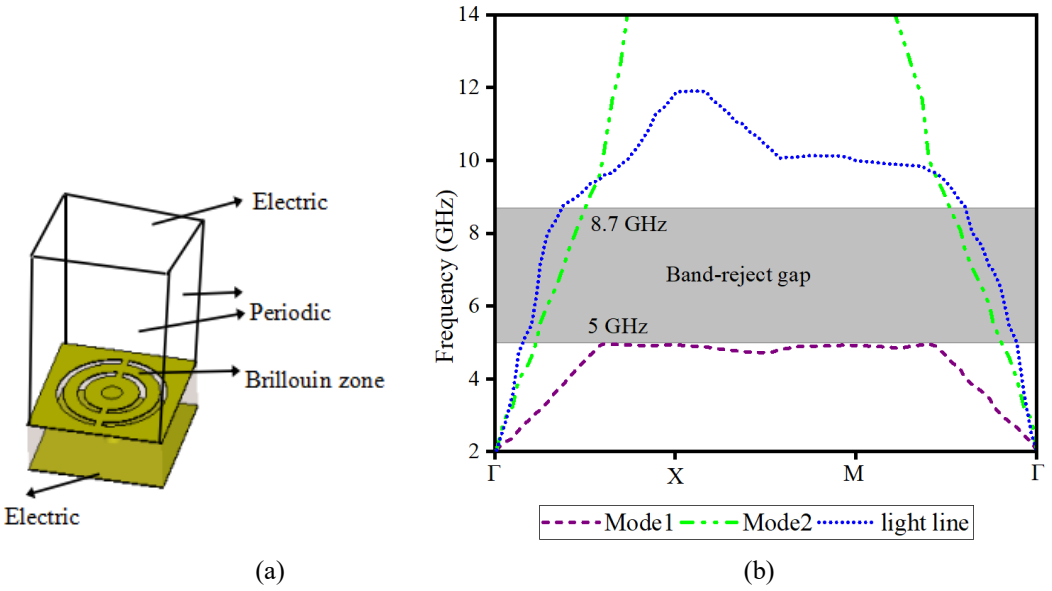

(a) (b)

FIGURE 5. Stopband analysis of mushroom-type EBG structure: (a) configuration of the unit cell, and (b) the simulated surface-wave dispersion diagram showing the bandgap region.

$$c_2 = \frac{\varepsilon_0 \varepsilon_r w'}{\pi} \operatorname{arch}\left(\frac{\sinh\left(\pi(w'+g)/4h\right)}{\sinh\left(\pi g/4h\right)}\right) \tag{5}$$

$$L = \mu_0 h\left\{\frac{1}{\pi}\left[\ln\left(\frac{a+\sqrt{a^2-(2r)^2}}{2r}\right)+\ln\ 2^{1/2}\right]\right\} \tag{6}$$

$$f_0 = \frac{1}{2\pi\sqrt{LC}} \tag{7}$$

where $w' \approx (1-2S/W^2)W, S = \pi r^2, a = W+g, C = C_1 + C_2$, where S represents the cross-sectional area of via hole; μ_0 is the permeability of free space; and ε_0 is the permittivity of free space. The initial unit cell parameters are computed using Equations (4)-(7) based on the target frequency bands of 5.05.21 GHz and $7.13-8.58$GHz. A dispersion diagram was generated to examine the high impedance characteristics of the EBG structure. Based on the initial parameters, the surface wave propagation within the EBG unit cell was analyzed. The side walls were assigned periodic boundary conditions, while the top and bottom surfaces were treated as perfect conductors, as depicted in Figure 5(a). The optimized EBG unit cell dimensions were set to $r_1 = 0.8$ mm, $r_2 = 1.6$ mm, $W = 4.0$ mm, and $g = 0.2$ mm to cover $5.0-5.21$GHz and $7.13-8.58$GHz frequency bands. The dispersion $(k-\beta)$ characteristics of the surface modes were obtained as shown in Figure 5(b). A distinct band-stop region between the first (TM0) and second (TE1) modes was observed across $5.0-8.58$GHz. In this context, Γ, X, and M represent symmetry points within the irreducible Brillouin zone, where $\Gamma - X$ corresponds to $\beta_x a/\pi$ at $\beta_x = 0; X-M$ corresponds to $\beta_x a/\pi$ at $\beta_x = \pi/a$; and $M-\Gamma$ corresponds to $\beta_x a/\pi$ when $\beta_x = \beta_x[11-14]$. Considering the slow-wave propagation characteristics of the surface modes, the dispersion curves lie below the light lines. The band-stop region extending from 5.0 to 8.58 GHz enhances the isolation between parallel antenna elements from 20 dB to 22.5 dB when a 3×3EBG array is placed at the center of the substrate, as illustrated in Figure 6(a).

3. Results and Performance Evaluation of the experiment.

The results of the proposed antenna were experimentally characterized using extensive experimental characterization. Basic parameters like scattering parameters (S-parameters), realized gain and radiation properties were also measured very carefully. A calibrated vector network analyzer over a wide frequency range was used to measure the reflection and transmission coefficients. The measurements of the radiation patterns and gain were done in a fully anechoic chamber in order to study the far-field behavior in absence of reflections. These measurements have been performed over the desired ultra-wideband frequency range to check the consistency with simulation results. The calculations of the antenna geometry were done to optimize the geometry of the antenna and predict its behavior before fabrication by applying a three-dimensional numerical solver to the full-wave electromagnetic. The prototype of the fabricated quad-port UWB-MIMO antenna that was in the experimental validation is illustrated in Figure 7.

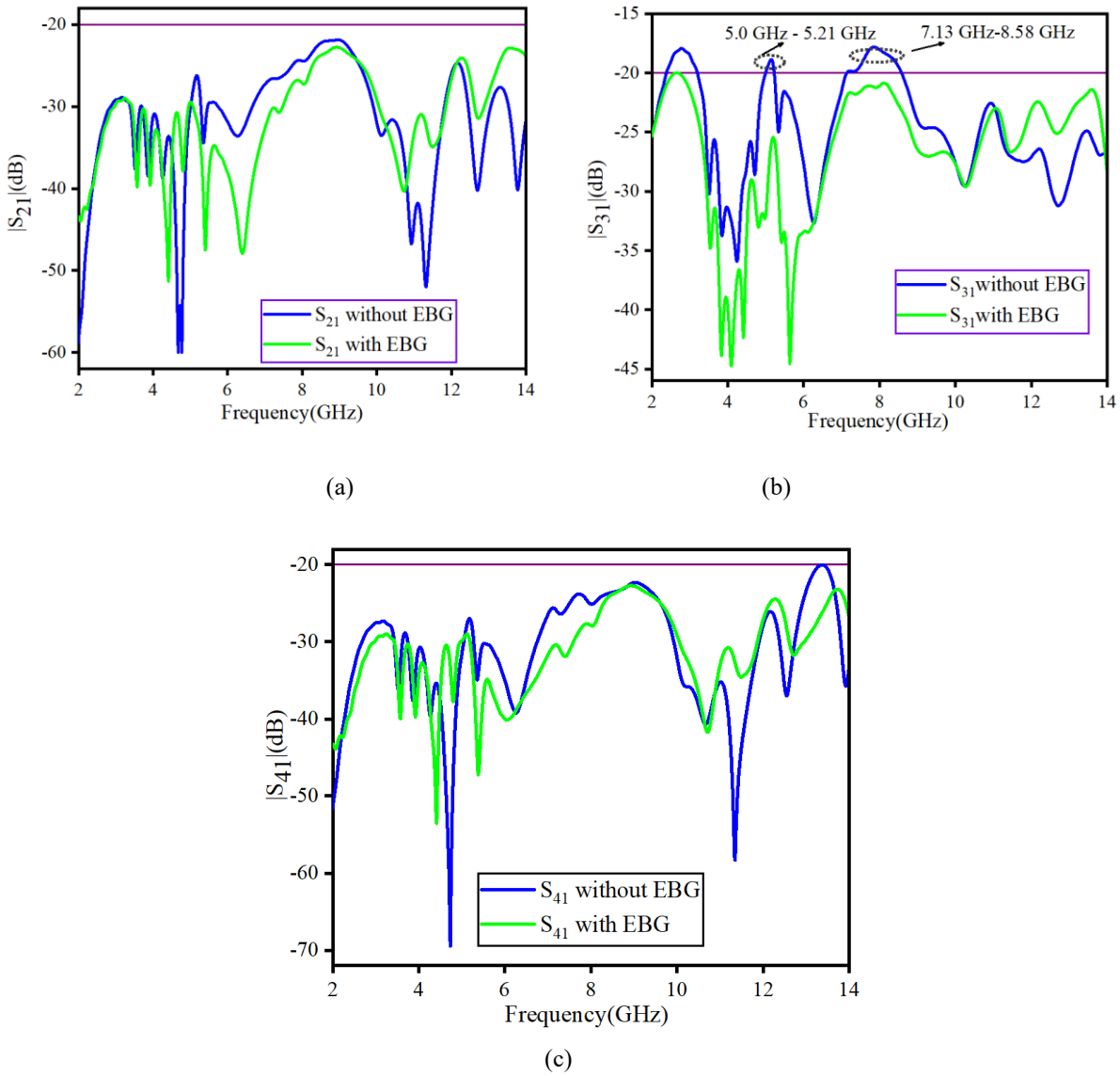

FIGURE 6. Comparison of simulated inter-element isolation with and without EBG integration: (a) transmission coefficient S31 between parallel elements, (b) S21 between orthogonal elements and (c) S41 between pairs of diagonal elements.

The proposed antenna has a continuous impedance bandwidth of between 3.0 GHz to 14.0 GHz which includes five defined rejection bands to allow WiMAX, C-band satellite links, Wi-Fi, INSAT and WLAN systems to pass

through them as shown in Figure 8. This isolation performance of the quad-port UWB-MIMO was measured using the transmission coefficients S21, S31, and S41. The results of the comparison between the simulated and measured results, as shown in Figure 8 show that the mutual coupling is below -22.5 dB across the entire frequency range of operation and it is observed that the antenna elements have been successfully decoupled. There are observed slight differences between simulation and measurement, which can be explained by more practical reasons of fabrication inaccuracies, connector and soldering effects, deviations of the substrate dielectric properties, and inevitable uncertainties of the experimental structure.

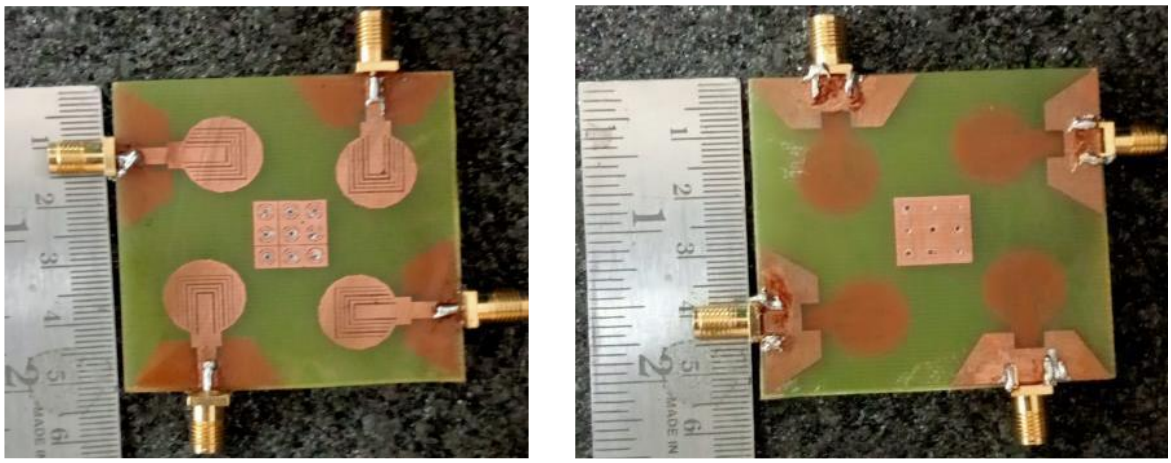

(a) (b)

FIGURE 7. Image of the designed prototype of the quad-port UWB-MIMO antenna: (a) top-layer (radiating side) and (b) bottom-layer (ground plane) images.

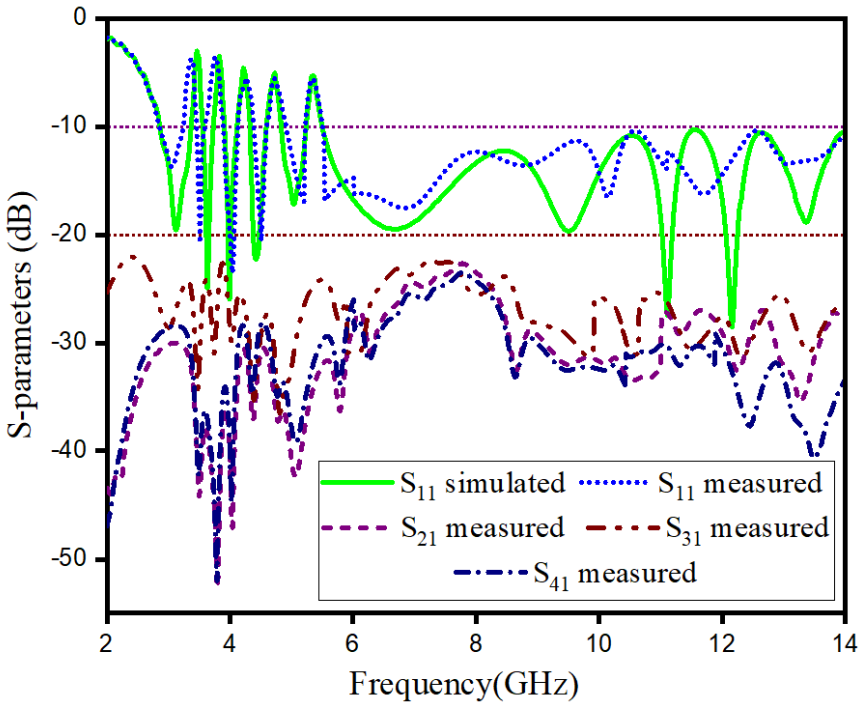

FIGURE 8. The characteristics of the proposed quad-port UWB-MIMO antenna in simulated and measured parts were in the form of scattering parameters.

3.1. Gain Characteristics and Radiation Behavior

Figure 9 gives the far-field radiation properties of the proposed antenna at the selected frequencies of 4 GHz, 7 GHz and 10 GHz. Radiation patterns were measured over both principal E-plane and H-plane to determine stability of the pattern over UWB operating range. The co-polarized radiation has bright lobes in the broadside direction in the E-plane and the cross-polarized components are also greatly suppressed. The polarization discrimination of the main radiation direction at the frequencies studied is more than 15 dB, which shows high levels of purity of the polarization of linear and directional stability. The H-plane patterns, on the other hand, exhibit almost omnidirectional properties, which are favorable to portable wireless devices. In this plane the cross-polarized levels are always low at all the frequencies that have been tested. In addition, it is observed that polarization isolation in the H-plane is above 20 dB, which proves the existence of uniform radiation distribution and low polarization distortion. Comparison of the numerically predicted and experimental values of the peak gain response of the antenna at the different frequencies is presented in Figure 10 indicating a very close match of the theoretically predicted values and the experimental findings. Within the range of effective impedance bandwidth (3.0-14.0 GHz) (without the rejected bands), the gain achieved is in the range of about 1.0 dB to 4.1 dB. The gain values are also not large at the lower end of the frequency range (3.0-4.5 GHz) because the radiating element dimensions are electrically small. The gain is slowly increased with frequency, and this is an indication of higher radiation efficiency at higher frequencies.

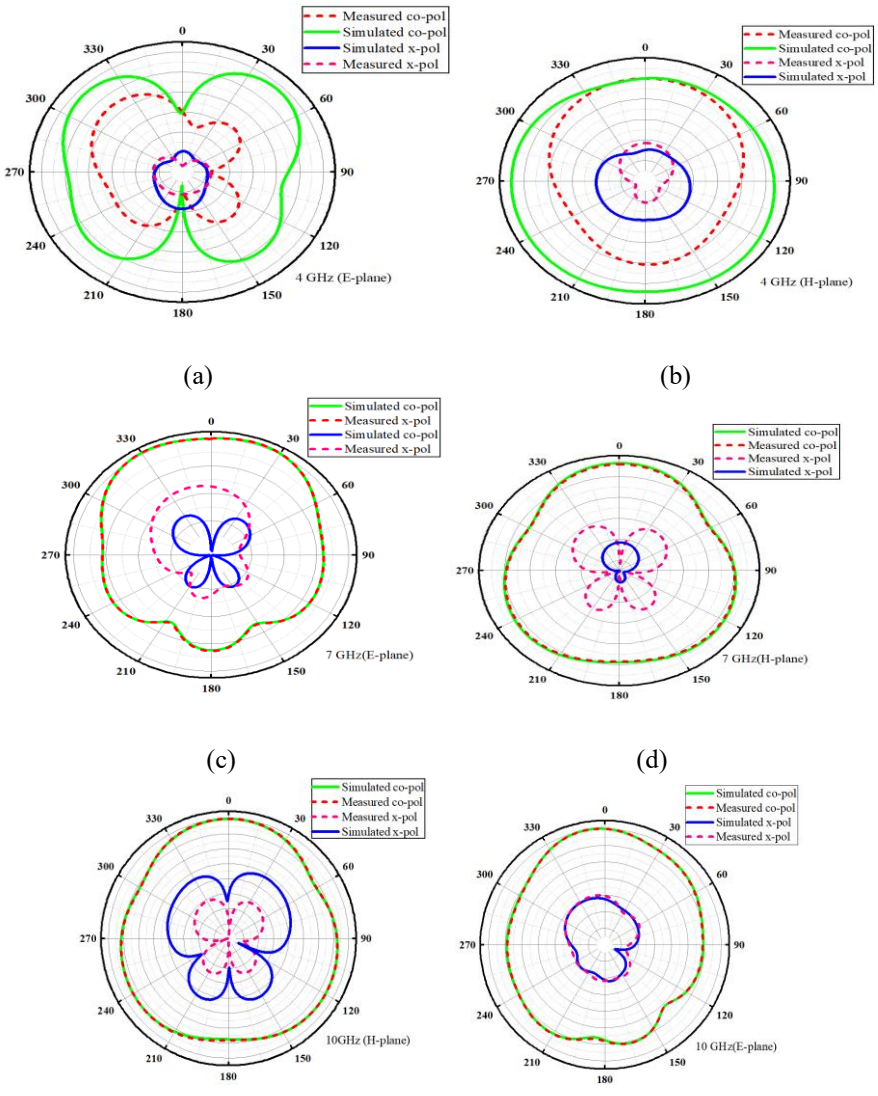

FIGURE 9. Computed and Experimental far-field radiation behavior of the proposed antenna at typical frequencies of 4 GHz, 7 GHz and 10 GHz.

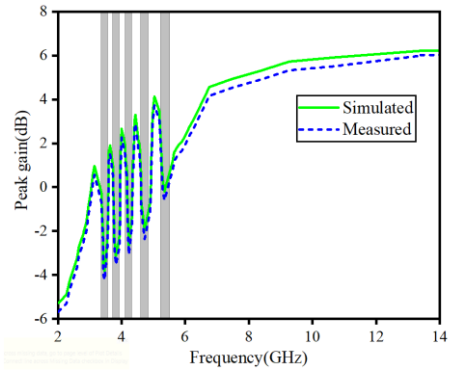

FIGURE 10. Simulated and measured peak realized gain of the proposed quad-port UWB-MIMO antenna over the operating band.

With a further increase in the operating frequency to 14.0 GHz, a significant improvement in the achieved gain can be noted which points to a higher radiation efficiency and increased power transfer at higher frequencies.

3.2. Diversity Evaluation Performance

MIMO antenna system diversity behavior is usually measured by a collection of performance parameters including envelope correlation coefficient (ECC), diversity gain (DG), radiation efficiency, channel capacity loss (CCL) and total active reflection coefficient (TARC). Among them, ECC is a very important factor in defining the level of interaction between the radiating elements. When the value of ECC is smaller, the correlation is weak and the diversity is enhanced. To ensure that the ECC is kept low to ensure the transmission of independent signal streams, it is desirable that it should be kept below 0.5 to ensure that the MIMO is operated in a practical and efficient manner. In multi-element systems, a three dimensional far-field radiation character of the antenna elements is used to compute a correlation coefficient (ρ_{eij}). This is assessed by the complex electric field components of the entire solid angle as formulated as following.

$$\rho_{eij} = \frac{\left|\int_0^{2\pi}\int_0^{\pi}\left(XPRE_{\theta i}E_{\theta j}^{*}P_{\theta} + E_{\varphi i}E_{\varphi j}^{*}P\varphi\right)d\Omega\right|^2}{\int_0^{2\pi}\int_0^{\pi}\left(XPRE_{\theta i}E_{\theta i}^{*}P_{\theta} + E_{\varphi i}E_{\varphi i}^{*}P\varphi\right)d\Omega} \times \int_0^{2\pi}\int_0^{\pi}\left(XPRE_{\theta j}E_{\theta j}^{*}P_{\theta} + E_{\varphi j}E_{\varphi j}^{*}P\varphi\right)d\Omega \tag{8}$$

Diversity gain (DG) is used to measure the increase in link reliability brought about by diversity operation in a MIMO system. It indicates the ability of the antenna to offer a constant signal strength at the presence of multiple propagation paths. DG value is calculated based on a standard mathematical formula which converts this value into the corresponding envelope correlation coefficient hence reflecting the overall performance of the antenna arrangement in terms of diversity performance.

$$DG = 10\sqrt{1 - ECC^2} \tag{9}$$

TABLE 1. Performance Comparison between the Proposed UWB-MIMO Antenna and the already reported designs.

Ref.	Antenna size (mm^2)	Bandwidth (GHz)	Gain (dB)	Isolation (dB)	ECC	CCL (bps/Hz)	TARC (dB)	No. of notches	No. of ports
[11]	39 × 39	2.3–13.75	4.6	> 22	< 0.02	< 0.2	< −10	3	4
[13]	30 × 30	3.1–11.0	5.0	> 20	< 0.02	< 0.35	< −10	1	2

[14]	23 × 29	3–12	5.9	> 15	< 0.15	NA	NA	NA	2
[16]	40 × 26	2.9–12.0	6.5	> 15	< 0.2	NA	NA	NA	2
[18]	24 × 31	3.4–12.1	4.4	> 16	< 0.001	NA	< −10	2	2
[24]	30 × 30	3.08–10.98	5	> 20	< 0.013	< 0.35	< −10	1	2
[25]	34 × 18	2.93–20.0	7.0	> 22	< 0.01	NA	< −20	2	2
[26]	38 × 38	3.0–15.0	5.0	> 15	< 0.15	< 0.4	NA	NA	4
[27]	24 × 40	2.9–12	5.0	> 23	< 0.2	NA	< −12	4	2
[28]	80 × 80	3–14	4.8	> 20	< 0.02	< 0.3	< −13	5	4
This work	54 × 54	3.0–14.0	6.2	> 22.5	< 0.02	< 0.2	< −10	5	4

The proposed UWB-MIMO antenna is simulated in figure 11(a) to obtain the envelope correlation coefficient (ECC) and diversity gain (DG). The values of the ECC are very low throughout the whole ultra-wideband spectrum where they are kept below 0.02 most of the spectrum. The ECC also exhibits a small increase with the intentionally created notch bands, even though it is lower than 0.05, indicating that mutual coupling and isolation between antenna elements are very weak. In line with this, the diversity gain is greater than 9.5 dB across the band passable, except in the rejected frequency bands, hence, corroborating good diversity performance, and consistent multi-path signal reception. The radiation efficiency features are represented in Figure 11(b). The antenna exhibits a high efficiency across the frequency range of operation where it is highest with a value of about 79.2 percent at 10 GHz. This is the maximum efficiency and it once again attests to the ability of the antenna to provide reliable MIMO operation. Figure 11(c) is the total active reflection coefficient (TARC) that is the effective reflection behavior of the antenna system when a number of ports (e.g. more than two) are excited at the same time. Throughout the band of functional operation, the TARC is lower than -10 dB with the notched frequencies being excluded where deliberate suppression of the signal is done. The channel capacity loss (CCL), that is used to measure the loss of data transmission capacity in MIMO systems, also remains within satisfactory ranges (usually less than 0 dB). All these findings agree with the fact that the proposed antenna has a low correlation, high efficiency and good multi-port capabilities within the required operating range.

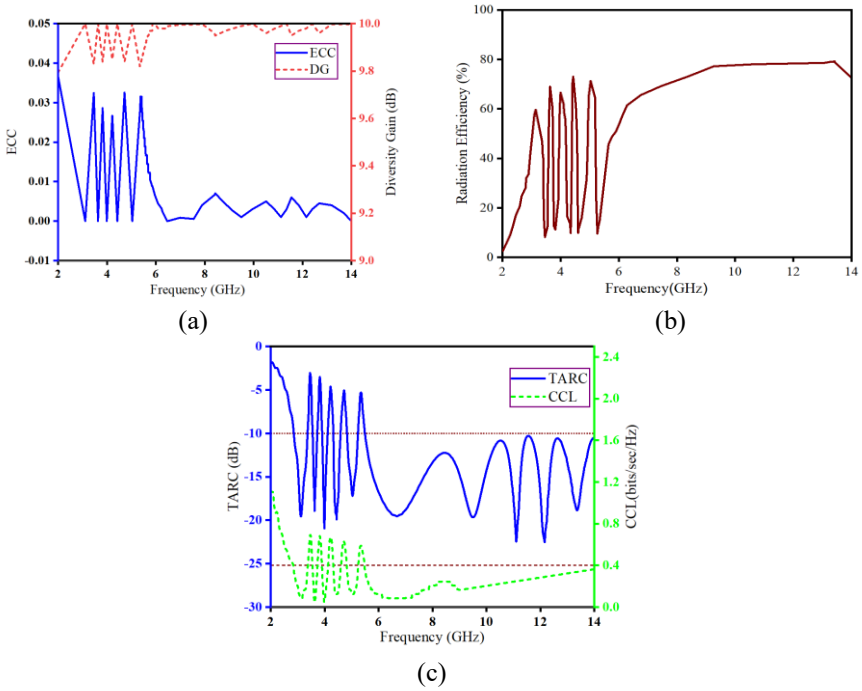

FIGURE 11. Diversity and MIMO performance values of the proposed antenna system: (a) Envelope Correlation Coefficient (ECC) and Diversity Gain (DG), (b) Radiation Efficiency, and (c) Channel Capacity Loss (CCL) and Total Active Reflection Coefficient (TARC).

3.3. Comparative Performance Analysis

Table 1 gives a comparative analysis of the proposed antenna and other UWB-MIMO antenna designs that have been reported recently in the literature. The comparative evaluation reveals the important parameters that performance can be evaluated including physical dimensions, impedance bandwidth, peak gain, isolation level, radiation properties, and diversity-related parameters. Based on the comparison, it can be seen that the proposed antenna provides an acceptable trade-off between small size, wide band of operation, increased gain, constant radiation pattern, and large element-to-element isolation. Besides, the antenna exhibits high MIMO diversity, which is manifested by low ECC, large diversity gains, low channel capacity loss (CCL) and good performance of TARC. Such findings verify the competitiveness and general performance efficiency of the suggested design in UWB-MIMO applications.

4. CONCLUSION

This paper presented a small quad-port UWB-MIMO antenna that is penta-band rejection and highly isolated with the addition of electromagnetic bandgap (EBG) structures. The suggested structure has a small volume of the 54 × 54 × 1.6 mm^3 and a broad band of impedance between 3 and 14 GHz. In this operating range, 5 different notched bands are achieved at 3.46, 3.82, 4.22, 4.72, and 5.34 GHz to work efficiently in suppressing the interference of WiMAX, C-band, Wi-Fi, INSAT and WLAN services. Better isolation between antenna elements is obtained by orthogonal positioning of radiators with strategically designed EBG structures which greatly decreases mutual coupling. The overall performance of the antenna has been confirmed by the detailed discussion of the most important parameters of MIMO diversity such as envelope correlation coefficient (ECC), diversity gain (DG), radiation efficiency, total active reflection coefficient (TARC) and channel capacity loss (CCL). The findings validate that it has low correlation, high efficiency, constant multi-port behavior, and good band-rejection behavior over the target frequency range. In general, the quad-element UWB-MIMO antenna designed exhibits high isolation, effective band-notch, and diversity properties. Due to its miniaturization and performance parameters, the antenna is most easily applied in the short-range, high-data-rate wireless systems including indoor UWB communication, gadget-to-gadget connections, and contemporary IoT-based systems. The inbuilt ability to suppress interference makes it reliable in locations where WLAN, WiMAX and sub-6 GHz 5G services overlap, which makes it a good prospective candidate in the portable, wearable, and smart electronic gadgets such as healthcare monitors and sensor-based communications units.

REFERENCES

[1] FCC, “Revision of part 15 of the commission’s rules regarding ultra-wideband transmission systems,” First Report and Order, ET Docket 98-153, 2002.

[2] Zhu, J., S. Li, B. Feng, L. Deng, and S. Yin, “Compact dual polarized UWB quasi-self-complementary MIMO/diversity antenna with band-rejection capability,” *IEEE Antennas and Wireless Propagation Letters*, Vol. 15, 905–908, 2016.

[3] Tripathi, S., A. Mohan, and S. Yadav, “A compact Koch fractal UWB MIMO antenna with WLAN band-rejection,” *IEEE Antennas and Wireless Propagation Letters*, Vol. 14, 1565–1568, 2015.

[4] Khan, M. K., Q. Feng, and Z. Zheng, “Experimental investigation and design of UWB MIMO antenna with enhanced isolation,” *Progress In Electromagnetics Research C*, Vol. 107, 287– 297, 2021.

[5] Khan, M. K. and Q. Feng, “Design validation of UWB MIMO antenna with enhanced isolation and novel strips for stop-band characteristics,” *Entropy*, Vol. 24, No. 6, 766, 2022.

[6] Navarro-Peralta, A. N., G. Leija-Hernández, and L. A. Iturri-Hinojosa, “Mutual coupling reduction between elements of UWB MIMO antenna using DGS enhancing the impedance bandwidth,” in *2023 IEEE International Autumn Meeting on Power, Electronics and Computing (ROPEC)*, 1–6, Ixtapa, Mexico, 2023.

[7] Ali, W. A. E. and A. A. Ibrahim, “A compact double-sided MIMO antenna with an improved isolation for UWB applications,” *AEU — International Journal of Electronics and Communications*, Vol. 82, 7–13, 2017.

[8] Urimubenshi, F., D. B. O. Konditi, J. de Dieu Iyakaremye, P. M. Mpele, and A. Munyaneza, "A novel approach for low mutual coupling and ultra-compact two port MIMO antenna development for UWB wireless application," *Heliyon*, Vol. 8, No. 3, e09057, 2022.

[9] Ding, K., C. Gao, D. Qu, and Q. Yin, "Compact broadband MIMO antenna with parasitic strip," *IEEE Antennas and Wireless Propagation Letters*, Vol. 16, 2349–2353, 2017.

[10] Khan, M. S., A.-D. Capobianco, A. I. Najam, I. Shoaib, E. Autizi and M. F. Shafique, "Compact ultra-wideband diversity antenna with a floating parasitic digitated decoupling structure," *IET Microwaves, Antennas & Propagation*, Vol. 8, No. 10, 747–753, Jul. 2014.

[11] Khan, M. S., A.-D. Capobianco, S. M. Asif, D. E. Anagnostou, R. M. Shubair, and B. D. Braaten, "A compact CSRR-enabled UWB diversity antenna," *IEEE Antennas and Wireless Propagation Letters*, Vol. 16, 808–812, 2016.

[12] Sipal, D., M. P. Abegaonkar, and S. K. Koul, "Easily extendable compact planar UWB MIMO antenna array," *IEEE Antennas and Wireless Propagation Letters*, Vol. 16, 2328–2331, 2017.

[13] Babu, S. R. andP. Dinesha, "Design of penta-band notched UWB MIMO antenna for diverse wireless applications," *Progress In Electromagnetics Research M*, Vol. 107, 35–49, 2022.

[14] Dabas, T., D. Gangwar, B. K. Kanaujia, and A. K. Gautam, "Mutual coupling reduction between elements of UWB MIMO antenna using small size uniplanar EBG exhibiting multiple stop bands," *AEU — International Journal of Electronics and Communications*, Vol. 93, 32–38, 2018.

[15] Markley, L. and G. V. Eleftheriades, "A negative-refractive index metamaterial for incident plane waves of arbitrary polarization," *IEEE Antennas and Wireless Propagation Letters*, Vol. 6, 28–32, 2007.

[16] Saritha, V., V. N. K. R. Devana, M. B. Lakshmi, M. A. Halimi, G. Devi, N. R. Lavuri, and A. J. A. Al-Gburi, "Low-profilefour-port MIMO antenna realizing penta-band notches for UWB systems," *Optik*, Vol. 336, 172454, 2024.

[17] Babu, S. R. and P. Dinesha, "Design and development of a miniaturized highly isolated UWB-MIMO diversity antenna with quad band notch characteristics," *Progress In Electromagnetics Research C*, Vol. 131, 197–208, 2023.

[18] Abbas, A., N. Hussain, M. A. Sufian, J. Jung, S. M. Park, and N. Kim, "Isolation and gain improvement of a rectangular notch UWB-MIMO antenna," *Sensors*, Vol. 22, No. 4, 1460, 2022.

[19] Biswal, S. P. and S. Das, "A low-profile dual port UWB-MIMO/diversity antenna with band rejection ability," *International Journal of RF and Microwave Computer-Aided Engineering*, Vol. 28, No. 1, e21159, 2018.

[20] Balanis, C. A., *Antenna Theory: Analysis and Design*, Chap. 14, 811–872, John Wiley & Sons, 2005.

[21] Assimonis, S. D., T. V. Yioultsis, and C. S. Antonopoulos, "Computational investigation and design of planar EBG structures for coupling reduction in antenna applications," *IEEE Transactions on Magnetics*, Vol. 48, No. 2, 771–774, 2012.

[22] Eltrass, A. S. and N. A. Elborae, "New design of UWB-MIMO antenna with enhanced isolation and dual-band rejection for WiMAX and WLAN systems," *IET Microwaves, Antennas & Propagation*, Vol. 13, No. 5, 683–691, 2019.

[23] Mchbal, A., N. A. Touhami, H. Elftouh, and A. Dkiouak, "Mutual coupling reduction using a protruded ground branch structure in a compact UWB owl-shaped MIMO antenna," *International Journal of Antennas and Propagation*, Vol. 2018, No. 1, 4598527, Sep. 2018.

[24] Chandel, R., A. K. Gautam, and K. Rambabu, "Design and packaging of an eye-shaped multiple-input–multiple-output antenna with high isolation for wireless UWB applications," *IEEE Transactions on Components, Packaging and Manufacturing Technology*, Vol. 8, No. 4, 635–642, Apr. 2018.

[25] Tang, Z., X. Wu, J. Zhan, S. Hu, Z. Xi, and Y. Liu, "Compact UWB-MIMO antenna with high isolation and triple band notched characteristics," *IEEE Access*, Vol. 7, 19 856–19 865, 2019.

[26] Liu, L., S. W. Cheung, and T. I. Yuk, "Compact MIMO antenna for portable devices in UWB applications," *IEEE Transactions on Antennas and Propagation*, Vol. 61, No. 8, 4257–4264, Aug.2013.

[27] Yang, F. and Y. Rahmat-Samii, "Microstrip antennas integrated with electromagnetic band-gap (EBG) structures: A low mutual coupling design for array applications," *IEEE Transactions on Antennas and Propagation*, Vol. 51, No. 10, 2936–2946, 2003.

[28] Kumar, P., T. Ali, and M. P. Mm, "Characteristic mode analysis based compact dual band-notched UWB MIMO antenna loaded with neutralization line," *Micromachines*, Vol. 13, No. 10, 1599, 2022.

[29] Chandel, R., A. K. Gautam, and K. Rambabu, "Tapered fed compact UWB MIMO-diversity antenna with dual band-notched characteristics," *IEEE Transactions on Antennas and Propagation*, Vol. 66, No. 4, 1677–1684, Apr. 2018.